TRANSPORT THEORY AND STATISTICAL PHYSICS, 30(2&3), 239–268 (2001)

THE P_N METHOD FOR CELL CALCULATIONS OF PLATE-TYPE FUEL ASSEMBLIES

A. D. Caldeira[1] and R. D. M. Garcia[1,2]

[1]Centro Técnico Aeroespacial, Instituto de Estudos Avançados, 12231-970 São José dos Campos, SP, Brazil
[2]HSH Scientific Computing, Rua Carlos de Campos, 286, 12242-540 São José dos Campos, SP, Brazil

ABSTRACT

An implementation of the P_N method for determining the effective multiplication factor and the neutron scalar flux and current in plate-type fuel cells is reported. Computational aspects of the method are discussed and numerical results are given for a three-region problem with group constants defined in a 64-group structure. The P_N results are found to agree quite well with results obtained using the ANISN code.

1. INTRODUCTION

Although the P_N method in its spatially continuous version [1–4] has been widely used for solving one-speed problems in neutron transport theory [5–18], there are relatively few reported applications of the method in the solution of multigroup problems [19–22]. It is noted that only one of these works [19] is devoted to multigroup criticality calculations, but at the

assembly level; there seems to be no reported application of the method to criticality problems at the cellular level. In this work, the spatially continuous version of the P_N method is further developed and used to determine the criticality condition and the corresponding neutron scalar flux and current for a plate-type fuel cell composed of any number of regions. The multigroup model is used and scattering anisotropy of arbitrary order is allowed.

The criticality condition considered in this work is that of determining the effective multiplication factor (k_{eff}) in the fuel region of the cell that gives rise to a stationary (and physically meaningful) neutron angular flux throughout the cell. In the case of the spatially continuous version of the P_N method, this reduces to finding the value of the (largest) multiplication factor k for which the determinant of a matrix that depends on the material composition and on the region dimensions of the cell vanishes. Once the effective multiplication factor is determined, the superposition coefficients of the P_N solutions in the material regions that constitute the cell can be evaluated by computing a vector in the null space of the critical matrix. Since the stationary scalar flux and current in the cell are, respectively, the Legendre moments of order zero and one of the angular flux, P_N approximations to these quantities can be easily computed once the superposition coefficients of the P_N solutions are available. One interesting feature of the proposed approach is that it provides an alternative to the approach used by existing numerical codes, which is based on the power method for generating the dominant eigenvalue and the corresponding eigenvector of a matrix.

To conclude this introduction, we note that even though the outlined approach looks straightforward to implement, various difficulties of computational nature had to be resolved before the procedure could be successfully applied to realistic (many-group) cell problems. Numerical results are given and compared with results of the ANISN code [23] for a three-region, 64-group cell problem to illustrate the capabilities of the method.

2. FORMULATION OF THE PROBLEM

We consider a plane cell composed of R distinct material regions as illustrated in Figure 1, where the boundaries z_0 and z_R are to be taken as reflective. Region 1 (the fuel) is multiplying and regions $2, 3, \ldots, R$ are nonmultiplying (e.g., fuel cladding, coolant, moderator, etc.). Considering G energy groups and Lth order anisotropic scattering, we follow the notation of Siewert [20] and write the neutron transport equation for

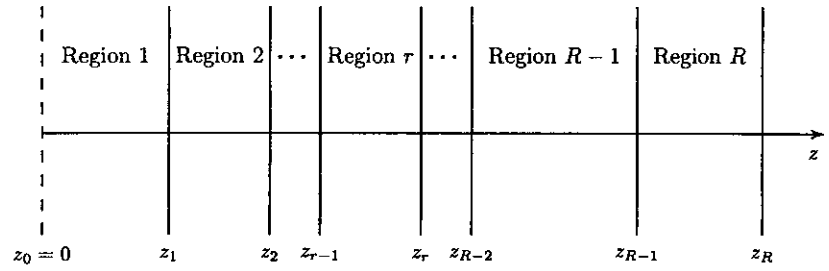

Figure 1. The cell geometry.

any region $1 \leq r \leq R$ as

$$\mu \frac{\partial}{\partial z} \mathbf{\Psi}_r(z, \mu) + \mathbf{S}_r \mathbf{\Psi}_r(z, \mu) = \frac{1}{2} \sum_{l=0}^{L} P_l(\mu) \mathbf{T}_{r,l} \int_{-1}^{1} P_l(\mu') \mathbf{\Psi}_r(z, \mu')\, d\mu', \tag{1}$$

where $\mathbf{\Psi}_r(z, \mu)$ is a column vector of dimension G having as components the group angular fluxes in region r, namely $\Psi_{r,1}(z, \mu), \Psi_{r,2}(z, \mu), \ldots, \Psi_{r,G}(z, \mu)$, $z \in (z_{r-1}, z_r)$ is the space variable measured in centimeters, and $\mu \in [-1, 1]$ is the cosine of the polar angle that specifies the direction of neutron travel. In addition, $\mathbf{S}_r$ is a diagonal matrix of order G with the group total cross sections $s_{r,1}, s_{r,2}, \ldots, s_{r,G}$ in the diagonal and $\mathbf{T}_{r,l}$ is the lth Legendre moment of the neutron transfer matrix whose (i,j) element is defined as

$$\sigma_{ij}^{r}(l) = \sigma_{s,ij}^{r}(l) + (1/k)\chi_i^r (\nu\sigma_f)_j^r \delta_{l,0}. \tag{2}$$

Here, $\sigma_{s,ij}^{r}(l)$ is the lth Legendre moment of the scattering transfer cross section from group j to group i, k is a factor to be determined so that a physically meaningful solution of Eq. (1) exists, $(\nu\sigma_f)_j^r$ is the group j average of the number of neutrons emitted per fission times the fission cross section and χ_i^r is the fraction of fission neutrons that appear in group i. Clearly, since in our problem multiplying material is present only in the fuel ($r = 1$) region of the cell, the second term on the right-hand side of Eq. (2) does not exist for $r = 2, 3, \ldots, R$. Moreover, the Kronecker delta in Eq. (2) indicates that we are considering the usual case of isotropic fission, but this is not a limitation of our approach.

To complete the formulation of the problem, we need to specify the boundary and interface conditions to which the vectors of group angular fluxes are subject. For the fuel ($r = 1$) region, the reflective boundary condition at $z = z_0 = 0$ can be expressed, for $\mu \geq 0$, as

$$\mathbf{\Psi}_1(0, \mu) = \mathbf{\Psi}_1(0, -\mu), \tag{3a}$$

while at each of the interfaces $z_r, r = 1, 2, \ldots, R-1$, we consider the continuity condition, for $\mu > 0$,

$$\Psi_r(z_r, \pm\mu) = \Psi_{r+1}(z_r, \pm\mu). \tag{3b}$$

Finally, the reflective condition at the outer boundary of the cell ($z = z_R$) can be expressed, for $\mu \geq 0$, as

$$\Psi_R(z_R, -\mu) = \Psi_R(z_R, \mu). \tag{3c}$$

We now discuss some general aspects of the P_N solution to Eq. (1) that are basic to our development.

3. GENERAL ASPECTS OF THE P_N SOLUTION

Following Siewert [20], we rewrite Eq. (1) in terms of an optical variable $\tau = z s_{\min,r}$, where $s_{\min,r}$ is the minimum of the group total cross sections in region r. This optical variable measures space in terms of the largest mean free path which, of course, varies from region to region. In spite of this, to keep our notation as simple as possible, in this section we drop, except when absolutely necessary, the index r that denotes the region. Thus, defining $\mathbf{\Sigma} = \mathbf{S}_r/s_{\min,r}$ and $\mathbf{C}_l = \mathbf{T}_{r,l}/s_{\min,r}$, we have, for $\tau \in (\tau_{r-1}, \tau_r)$,

$$\mu \frac{\partial}{\partial \tau} \mathbf{\Psi}(\tau, \mu) + \mathbf{\Sigma}\mathbf{\Psi}(\tau, \mu) = \frac{1}{2} \sum_{l=0}^{L} P_l(\mu) \mathbf{C}_l \int_{-1}^{1} P_l(\mu') \mathbf{\Psi}(\tau, \mu')\, d\mu'. \tag{4}$$

The P_N solution to Eq. (4) for N odd has been developed by Siewert [20]. It satisfies exactly the first $N+1$ moments of Eq. (4) and can be written as

$$\mathbf{\Psi}(\tau, \mu) = \frac{1}{2} \sum_{n=0}^{N} (2n+1) \mathbf{\Phi}_n(\tau) P_n(\mu), \tag{5}$$

where, with $J = G(N+1)/2$,

$$\mathbf{\Phi}_n(\tau) = \sum_{j=1}^{J} \left[A_j e^{-(\tau - \tau_{r-1})/\xi_j} + (-1)^n B_j e^{-(\tau_r - \tau)/\xi_j} \right] \mathbf{G}_n(\xi_j). \tag{6}$$

Here, the $\{A_j\}$ and $\{B_j\}$ are superposition coefficients of the P_N modes that need to be determined, $\{\mathbf{G}_n(\xi)\}$ are vectors of dimension G that satisfy

$$\xi \mathbf{h}_n \mathbf{G}_n(\xi) = (n+1)\mathbf{G}_{n+1}(\xi) + n\mathbf{G}_{n-1}(\xi), \tag{7}$$

with

$$\mathbf{h}_n = \begin{cases} (2n+1)\mathbf{\Sigma} - \mathbf{C}_n, & n \leq L, \\ (2n+1)\mathbf{\Sigma}, & n > L, \end{cases} \tag{8}$$

and the J pairs $\{\pm\xi_j\}$ – the so-called P_N eigenvalues – are the $2J$ values of ξ that satisfy the *truncation condition* $\mathbf{G}_{N+1}(\xi) = \mathbf{0}$. We note that here, as in a previous work on the P_N method for radiative transfer with polarization [24], we have observed that some of the P_N eigenvalues with absolute value < 1 may appear as complex quadruples. In addition, when the medium is multiplying, at least one pair of P_N eigenvalues turns out to be pure imaginary.

The calculation of the P_N eigenvalues and the required **G**-vectors can be reduced to solving the eigensystem [20, 25]

$$\mathbf{A}\mathbf{G}_e(\xi) = \xi^2 \mathbf{G}_e(\xi), \tag{9}$$

where the $J \times J$ matrix $\mathbf{A}$ is defined as

$$\mathbf{A} = \begin{pmatrix} \mathbf{Y}_0 & \mathbf{Z}_0 & \mathbf{0} & \ldots & \mathbf{0} & \mathbf{0} & \mathbf{0} \\ \mathbf{X}_2 & \mathbf{Y}_2 & \mathbf{Z}_2 & \ldots & \mathbf{0} & \mathbf{0} & \mathbf{0} \\ \mathbf{0} & \mathbf{X}_4 & \mathbf{Y}_4 & \ldots & \mathbf{0} & \mathbf{0} & \mathbf{0} \\ \vdots & \vdots & \vdots & \ddots & \vdots & \vdots & \vdots \\ \mathbf{0} & \mathbf{0} & \mathbf{0} & \ldots & \mathbf{Y}_{N-5} & \mathbf{Z}_{N-5} & \mathbf{0} \\ \mathbf{0} & \mathbf{0} & \mathbf{0} & \ldots & \mathbf{X}_{N-3} & \mathbf{Y}_{N-3} & \mathbf{Z}_{N-3} \\ \mathbf{0} & \mathbf{0} & \mathbf{0} & \ldots & \mathbf{0} & \mathbf{X}_{N-1} & \mathbf{Y}_{N-1} \end{pmatrix}, \tag{10}$$

with

$$\mathbf{X}_n = n(n-1)\mathbf{h}_n^{-1}\mathbf{h}_{n-1}^{-1}, \tag{11a}$$

$$\mathbf{Y}_n = n^2 \mathbf{h}_n^{-1}\mathbf{h}_{n-1}^{-1} + (n+1)^2 \mathbf{h}_n^{-1}\mathbf{h}_{n+1}^{-1} \tag{11b}$$

and

$$\mathbf{Z}_n = (n+1)(n+2)\mathbf{h}_n^{-1}\mathbf{h}_{n+1}^{-1}, \tag{11c}$$

and the vector $\mathbf{G}_e(\xi)$ of dimension J has the even **G**-vectors as components, i.e.

$$\mathbf{G}_e(\xi) = \begin{pmatrix} \mathbf{G}_0(\xi) \\ \mathbf{G}_2(\xi) \\ \vdots \\ \mathbf{G}_{N-1}(\xi) \end{pmatrix}. \tag{12}$$

Clearly, once the eigensystem expressed by Eq. (9) is solved, the required $\{\xi_j\}$ are found as the positive square roots of the eigenvalues and the even $\mathbf{G}_n(\xi_j)$, $n = 0, 2, \ldots, N-1$, are the vector components of the corresponding

eigenvectors, as specified by Eq. (12). Once the even **G**-vectors are available, the odd ones can be computed by using Eq. (7) with $n = 1, 3, \ldots, N$ and the truncation condition $\mathbf{G}_{N+1}(\xi_j) = \mathbf{0}$.

Alternatively, it is possible to formulate the problem of computing the P_N eigenvalues in terms of the odd **G**-vectors. Thus, instead of solving the eigensystem defined by Eq. (9), we can solve [20]

$$\mathbf{B}\mathbf{G}_o(\xi) = \xi^2 \mathbf{G}_o(\xi), \tag{13}$$

where the $J \times J$ matrix **B** is defined as

$$\mathbf{B} = \begin{pmatrix} \mathbf{Y}_1 & \mathbf{Z}_1 & \mathbf{0} & \ldots & \mathbf{0} & \mathbf{0} & \mathbf{0} \\ \mathbf{X}_3 & \mathbf{Y}_3 & \mathbf{Z}_3 & \ldots & \mathbf{0} & \mathbf{0} & \mathbf{0} \\ \mathbf{0} & \mathbf{X}_5 & \mathbf{Y}_5 & \ldots & \mathbf{0} & \mathbf{0} & \mathbf{0} \\ \vdots & \vdots & \vdots & \ddots & \vdots & \vdots & \vdots \\ \mathbf{0} & \mathbf{0} & \mathbf{0} & \ldots & \mathbf{Y}_{N-4} & \mathbf{Z}_{N-4} & \mathbf{0} \\ \mathbf{0} & \mathbf{0} & \mathbf{0} & \ldots & \mathbf{X}_{N-2} & \mathbf{Y}_{N-2} & \mathbf{Z}_{N-2} \\ \mathbf{0} & \mathbf{0} & \mathbf{0} & \ldots & \mathbf{0} & \mathbf{X}_N & \mathbf{Y}'_N \end{pmatrix}, \tag{14}$$

with

$$\mathbf{Y}'_N = N^2 \mathbf{h}_N^{-1} \mathbf{h}_{N-1}^{-1}, \tag{15}$$

and the vector $\mathbf{G}_o(\xi)$ of dimension J has the odd **G**-vectors as components, i.e.

$$\mathbf{G}_o(\xi) = \begin{pmatrix} \mathbf{G}_1(\xi) \\ \mathbf{G}_3(\xi) \\ \vdots \\ \mathbf{G}_N(\xi) \end{pmatrix}. \tag{16}$$

Once the eigensystem defined by Eq. (13) is solved, the required even **G**-vectors can be computed by using Eq. (7) with $n = 0, 2, \ldots, N-1$.

We have used subroutines BALANC, ELMHES, ELTRAN, HQR2 and BALBAK of the EISPACK package [26] to solve both of the eigensystems defined by Eqs. (9) and (13), in the context of the test problem discussed in Section 6. We have concluded that the accuracies of the eigenvalues and eigenvectors obtained by solving both of these eigensystems are similar.

4. THE P_N SOLUTION FOR THE CELL PROBLEM

In this section, we specialize the general P_N solution discussed in Section 3 to each of the material regions that constitute the cell and use

the boundary and interface conditions of Section 2 to develop a system of homogeneous equations for the unknown superposition coefficients of the P_N solutions. As we will see, the condition for which nontrivial solutions to that system of equations are found to exist, coupled with the requirement that only one of these solutions is of physical interest (if more than one exists), determines the desired effective multiplication factor (k_{eff}) of the cell.

4.1. The Solution for the Fuel Region

In terms of the optical variable introduced in the beginning of Section 3, the fuel region is defined by $\tau \in (0, \tau_1)$, where $\tau_1 = z_1 s_{\min,1}$. Here z_1 represents the half-thickness of the fuel plate in cm (see Figure 1) and $s_{\min,1}$ is the minimum of the group total cross sections in the fuel.

In the case of the fuel region, it turns out that the reflective boundary condition expressed by Eq. (3a) can be used to relate the $\{B_j\}$ coefficients in Eq. (6) to the $\{A_j\}$ coefficients. Thus, after introducing an exponential rescaling of the $\{A_j\}$ coefficients to avoid destructive overflows in our computational implementation, we can specialize Eqs. (5) and (6) for the fuel region as

$$\mathbf{\Psi}_1(\tau, \mu) = \frac{1}{2} \sum_{n=0}^{N} (2n+1) \mathbf{\Phi}_{1,n}(\tau) P_n(\mu) \tag{17}$$

and

$$\begin{aligned} \mathbf{\Phi}_{1,n}(\tau) = & \sum_{j=1}^{J_1} A_{1,j} \mathbf{Z}^-_{1,n}(\tau, \xi_{1,j}) \\ & + \sum_{j=J_1+1}^{J_S} A_{1,j} \left[e^{-(\tau_1+\tau)/\xi_{1,j}} + (-1)^n e^{-(\tau_1-\tau)/\xi_{1,j}} \right] \mathbf{G}_{1,n}(\xi_{1,j}) \\ & + \sum_{\substack{j=J_S+1 \\ \Delta j=2}}^{J-1} \left\{ A_{1,j} \left[e^{-\lambda_{1,j}(\tau_1+\tau)/(\xi_{1,j}\tilde{\xi}_{1,j})} \mathbf{Z}^-_{1,n}(\tau, \xi_{1,j}) \right. \right. \\ & \left. + (-1)^n e^{-\lambda_{1,j}(\tau_1-\tau)/(\xi_{1,j}\tilde{\xi}_{1,j})} \mathbf{Z}^+_{1,n}(\tau, \xi_{1,j}) \right] \\ & + A_{1,j+1} \left[e^{-\lambda_{1,j}(\tau_1+\tau)/(\xi_{1,j}\tilde{\xi}_{1,j})} \mathbf{W}^+_{1,n}(\tau, \xi_{1,j}) \right. \\ & \left. \left. - (-1)^n e^{-\lambda_{1,j}(\tau_1-\tau)/(\xi_{1,j}\tilde{\xi}_{1,j})} \mathbf{W}^-_{1,n}(\tau, \xi_{1,j}) \right] \right\}. \end{aligned} \tag{18}$$

To write Eq. (18) in the way we did here, we have assumed that the P_N eigenvalues are ordered so that the eigenvalues $\xi_{1,j} = i\eta_{1,j}$, $j = 1, 2, \ldots, J_I$, are pure imaginary, the eigenvalues $\xi_{1,j}$, $j = J_I + 1, J_I + 2, \ldots, J_S$, are real, and the eigenvalue pairs $(\xi_{1,j}, \bar{\xi}_{1,j})$, $j = J_S + 1, J_S + 3, \ldots, J - 1$, with $\xi_{1,j} = \lambda_{1,j} + i\eta_{1,j}$, are complex conjugate. We note that the restriction $\Delta j = 2$ attached to the third summation symbol on the right-hand side of Eq. (18) means that j is to be incremented by 2 in that summation. In addition, we have used the general definitions

$$\mathbf{Z}^{\pm}_{r,n}(\tau, \xi) = \cos[\eta\tau/(\xi\bar{\xi})]\,\Re\{\mathbf{G}_{r,n}(\xi)\} \pm \sin[\eta\tau/(\xi\bar{\xi})]\,\Im\{\mathbf{G}_{r,n}(\xi)\} \tag{19}$$

and

$$\mathbf{W}^{\pm}_{r,n}(\tau, \xi) = \sin[\eta\tau/(\xi\bar{\xi})]\,\Re\{\mathbf{G}_{r,n}(\xi)\} \pm \cos[\eta\tau/(\xi\bar{\xi})]\,\Im\{\mathbf{G}_{r,n}(\xi)\} \tag{20}$$

to write Eq. (18) in its present form.

4.2. The Solution for an Intermediate Region

For an intermediate region $2 \le r \le R - 1$, defined by $\tau \in (\tau_{r-1}, \tau_r)$, where $\tau_x = \sum_{i=1}^{x}(z_i - z_{i-1})s_{\min,i}$ for $x = r - 1$ or r, we rewrite the P_N solution expressed by Eqs. (5) and (6) as

$$\mathbf{\Psi}_r(\tau, \mu) = \frac{1}{2}\sum_{n=0}^{N}(2n + 1)\mathbf{\Phi}_{r,n}(\tau)P_n(\mu), \tag{21}$$

with

$$\begin{aligned}\mathbf{\Phi}_{r,n}(\tau) = {} & \sum_{j=1}^{J_R}\left[A_{r,j}e^{-(\tau-\tau_{r-1})/\xi_{r,j}} + (-1)^n B_{r,j}e^{-(\tau_r-\tau)/\xi_{r,j}}\right]\mathbf{G}_{r,n}(\xi_{r,j}) \\ & + \sum_{\substack{j=J_R+1 \\ \Delta j=2}}^{J-1}\left\{\left[A_{r,j}\mathbf{Z}^{-}_{r,n}(\tau - \tau_{r-1}, \xi_{r,j}) + A_{r,j+1}\mathbf{W}^{+}_{r,n}(\tau - \tau_{r-1}, \xi_{r,j})\right]\right. \\ & \times e^{-\lambda_{r,j}(\tau-\tau_{r-1})/(\xi_{r,j}\bar{\xi}_{r,j})} \\ & + (-1)^n\left[B_{r,j}\mathbf{Z}^{-}_{r,n}(\tau_r - \tau, \xi_{r,j}) + B_{r,j+1}\mathbf{W}^{+}_{r,n}(\tau_r - \tau, \xi_{r,j})\right] \\ & \left.\times e^{-\lambda_{r,j}(\tau_r-\tau)/(\xi_{r,j}\bar{\xi}_{r,j})}\right\}.\end{aligned} \tag{22}$$

Here we have assumed that $\xi_{r,j}$, $j = 1, 2, \ldots, J_R$, are real eigenvalues and that $(\xi_{r,j}, \bar{\xi}_{r,j})$, $j = J_R + 1, J_R + 3, \ldots, J - 1$, with $\xi_{r,j} = \lambda_{r,j} + i\eta_{r,j}$, are complex conjugate pairs.

4.3. The Solution for the Outermost Region

For the outermost ($r = R$) region of the cell, defined by $\tau \in (\tau_{R-1}, \tau_R)$, where $\tau_x = \sum_{i=1}^{x}(z_i - z_{i-1})s_{\min,i}$ for $x = R - 1$ or R, we use the reflective boundary condition expressed by Eq. (3c) to relate the $\{B_j\}$ coefficients in Eq. (6) to the $\{A_j\}$ coefficients. Thus, we find that we can write Eqs. (5) and (6) for the outermost region as

$$\mathbf{\Psi}_R(\tau, \mu) = \frac{1}{2}\sum_{n=0}^{N}(2n + 1)\mathbf{\Phi}_{R,n}(\tau)P_n(\mu) \tag{23}$$

and

$$\begin{aligned}\mathbf{\Phi}_{R,n}(\tau) = {} & \sum_{j=1}^{J_R}A_{R,j}\left[e^{-(\tau-\tau_{R-1})/\xi_{R,j}} + (-1)^n e^{-(2\tau_R-\tau_{R-1}-\tau)/\xi_{R,j}}\right]\mathbf{G}_{R,n}(\xi_{R,j}) \\ & + \sum_{\substack{j=J_R+1 \\ \Delta j=2}}^{J-1}\left\{\left[A_{R,j}\mathbf{Z}^{-}_{R,n}(\tau - \tau_{R-1}, \xi_{R,j}) + A_{R,j+1}\mathbf{W}^{+}_{R,n}(\tau - \tau_{R-1}, \xi_{R,j})\right]\right. \\ & \times e^{-\lambda_{R,j}(\tau-\tau_{R-1})/(\xi_{R,j}\bar{\xi}_{R,j})} \\ & + (-1)^n\left[A_{R,j}\mathbf{Z}^{-}_{R,n}(2\tau_R - \tau_{R-1} - \tau, \xi_{R,j})\right. \\ & \left.\left. + A_{R,j+1}\mathbf{W}^{+}_{R,n}(2\tau_R - \tau_{R-1} - \tau, \xi_{R,j})\right]e^{-\lambda_{R,j}(2\tau_R-\tau_{R-1}-\tau)/(\xi_{R,j}\bar{\xi}_{R,j})}\right\}.\end{aligned} \tag{24}$$

As before, we have assumed that $\xi_{R,j}$, $j = 1, 2, \ldots, J_R$, are real eigenvalues and that $(\xi_{R,j}, \bar{\xi}_{R,j})$, $j = J_R + 1, J_R + 3, \ldots, J - 1$, with $\xi_{R,j} = \lambda_{R,j} + i\eta_{R,j}$, are complex conjugate pairs.

4.4. Application of the Interface Conditions

Having used the reflective boundary conditions expressed by Eqs. (3a) and (3c) to eliminate half of the superposition coefficients for the fuel and the outermost regions, we still have $2J(R - 1)$ unknown coefficients in our P_N solutions: the $\{A_{1,j}\}$ in Eq. (18), the $\{A_{r,j}\}$ and $\{B_{r,j}\}$ for $r = 2, 3, \ldots, R - 1$ in Eq. (22), and the $\{A_{R,j}\}$ in Eq. (24). We thus need to generate the same number of approximate conditions from the interface conditions expressed by Eq. (3b) to be able to determine these coefficients. For this purpose, we elected to use the Mark prescription [1] of selecting

approximate boundary or interface conditions for the P_N method, and so, denoting as $\{\mu_i\}$ the $(N+1)/2$ *positive* zeros of the Legendre polynomial $P_{N+1}(\mu)$, we impose that the following interface conditions be satisfied at τ_r, $r = 1, 2, \ldots, R-1$:

$$\Psi_r(\tau_r, \pm\mu_i) = \Psi_{r+1}(\tau_r, \pm\mu_i). \tag{25}$$

For convenience, instead of using the set of approximate interface conditions expressed by Eq. (25), we prefer to combine these equations as

$$\Psi_r(\tau_r, \mu_i) \pm \Psi_r(\tau_r, -\mu_i) = \Psi_{r+1}(\tau_r, \mu_i) \pm \Psi_{r+1}(\tau_r, -\mu_i), \tag{26}$$

for $r = 1, 2, \ldots, R-1$, and substitute the P_N solutions expressed by Eqs. (17), (18), (21)–(24) into Eqs. (26) to obtain, for the interface τ_1,

$$\mathbf{C}\mathbf{A}_1 - \mathbf{U}_2\mathbf{A}_2 - \mathbf{V}_2\mathbf{B}_2 = \mathbf{0} \tag{27a}$$

and

$$\mathbf{D}\mathbf{A}_1 + \mathbf{R}_2\mathbf{A}_2 - \mathbf{S}_2\mathbf{B}_2 = \mathbf{0}, \tag{27b}$$

for the interfaces τ_r, $r = 2, 3, \ldots, R-2$,

$$\mathbf{V}_r\mathbf{A}_r + \mathbf{U}_r\mathbf{B}_r - \mathbf{U}_{r+1}\mathbf{A}_{r+1} - \mathbf{V}_{r+1}\mathbf{B}_{r+1} = \mathbf{0} \tag{27c}$$

and

$$\mathbf{S}_r\mathbf{A}_r - \mathbf{R}_r\mathbf{B}_r - \mathbf{R}_{r+1}\mathbf{A}_{r+1} + \mathbf{S}_{r+1}\mathbf{B}_{r+1} = \mathbf{0}, \tag{27d}$$

and, for the interface τ_{R-1},

$$\mathbf{V}_{R-1}\mathbf{A}_{R-1} + \mathbf{U}_{R-1}\mathbf{B}_{R-1} - \mathbf{E}\mathbf{A}_R = \mathbf{0} \tag{27e}$$

and

$$\mathbf{S}_{R-1}\mathbf{A}_{R-1} - \mathbf{R}_{R-1}\mathbf{B}_{R-1} - \mathbf{F}\mathbf{A}_R = \mathbf{0}. \tag{27f}$$

Here, the vectors $\mathbf{A}_r$, $r = 1, 2, \ldots, R$, and $\mathbf{B}_r$, $r = 2, 3, \ldots, R-1$, are all of dimension J and have the unknown coefficients of the P_N solutions as components, i.e.

$$\mathbf{A}_r = \begin{pmatrix} A_{r,1} \\ A_{r,2} \\ \vdots \\ A_{r,J} \end{pmatrix} \quad \text{and} \quad \mathbf{B}_r = \begin{pmatrix} B_{r,1} \\ B_{r,2} \\ \vdots \\ B_{r,J} \end{pmatrix}, \tag{28a and b}$$

and the $J \times J$ submatrices $\mathbf{C}$, $\mathbf{D}$, $\mathbf{E}$, $\mathbf{F}$, and $\mathbf{U}_r$, $\mathbf{V}_r$, $\mathbf{R}_r$, $\mathbf{S}_r$, $r = 2, 3, \ldots, R-1$, are defined in Appendix A.

In passing, we note that the fact that we used Eq. (26) instead of Eq. (25) to establish the Mark version of the interface conditions to be satisfied by our P_N solutions allowed us to cut by half the computational

work required to calculate the elements of these submatrices (see explanation at the end of Appendix A).

Equations (27a) to (27f) can now be written as a homogeneous system of order $2J(R-1)$, viz.

$$\mathbf{M}\mathbf{X} = \mathbf{0}, \tag{29}$$

where

$$\mathbf{M} = \begin{pmatrix} \mathbf{C} & -\mathbf{U}_2 & -\mathbf{V}_2 & \mathbf{0} & \mathbf{0} & \mathbf{0} & \cdots & \mathbf{0} & \mathbf{0} \\ \mathbf{D} & \mathbf{R}_2 & -\mathbf{S}_2 & \mathbf{0} & \mathbf{0} & \mathbf{0} & \cdots & \mathbf{0} & \mathbf{0} \\ \mathbf{0} & \mathbf{V}_2 & \mathbf{U}_2 & -\mathbf{U}_3 & -\mathbf{V}_3 & \mathbf{0} & \cdots & \mathbf{0} & \mathbf{0} \\ \mathbf{0} & \mathbf{S}_2 & -\mathbf{R}_2 & -\mathbf{R}_3 & \mathbf{S}_3 & \mathbf{0} & \cdots & \mathbf{0} & \mathbf{0} \\ \vdots & \vdots & \ddots & \ddots & \ddots & \ddots & \ddots & \vdots & \vdots \\ \mathbf{0} & \mathbf{0} & \cdots & \mathbf{0} & \mathbf{V}_{R-2} & \mathbf{U}_{R-2} & -\mathbf{U}_{R-1} & -\mathbf{V}_{R-1} & \mathbf{0} \\ \mathbf{0} & \mathbf{0} & \cdots & \mathbf{0} & \mathbf{S}_{R-2} & -\mathbf{R}_{R-2} & -\mathbf{R}_{R-1} & \mathbf{S}_{R-1} & \mathbf{0} \\ \mathbf{0} & \mathbf{0} & \cdots & \mathbf{0} & \mathbf{0} & \mathbf{0} & \mathbf{V}_{R-1} & \mathbf{U}_{R-1} & -\mathbf{E} \\ \mathbf{0} & \mathbf{0} & \cdots & \mathbf{0} & \mathbf{0} & \mathbf{0} & \mathbf{S}_{R-1} & -\mathbf{R}_{R-1} & -\mathbf{F} \end{pmatrix} \tag{30}$$

and

$$\mathbf{X} = \begin{pmatrix} \mathbf{A}_1 \\ \mathbf{A}_2 \\ \mathbf{B}_2 \\ \mathbf{A}_3 \\ \vdots \\ \mathbf{B}_{R-2} \\ \mathbf{A}_{R-1} \\ \mathbf{B}_{R-1} \\ \mathbf{A}_R \end{pmatrix}. \tag{31}$$

Clearly, since a homogeneous system has a nontrivial solution only if the determinant of the corresponding matrix of coefficients vanishes, this is the criticality condition that allows us to find k_{eff}, the (largest) value of k in Eq. (2) that gives rise to a physically meaningful solution of Eq. (1). Moreover, a vector $\mathbf{X} \neq \mathbf{0}$ in the null space of the critical matrix $\mathbf{M}$ yields a set of vectors $\mathbf{A}_r$, $r = 1, 2, \ldots, R$, and $\mathbf{B}_r$, $r = 2, \ldots, R-1$, that satisfy Eqs. (27a) to (27f). Once these vectors are available, all of the superposition coefficients in the P_N solutions become known, up to a normalization factor that can be freely chosen.

Finally, we note that the zeroth and first Legendre moments expressed by Eqs. (18), (22) and (24) with $n = 0$ and $n = 1$ yield the desired

P_N approximations to the scalar flux and current vectors in the fuel, intermediate and outermost regions, respectively.

5. COMPUTATIONAL ASPECTS OF THE P_N SOLUTION

In this section, we discuss in detail what we believe to be the most relevant aspects of our computational implementation of the P_N solution reported in Section 4. We also report an alternative (and more economical) way of implementing our solution.

5.1. Computational Implementation

We begin with the determination of k_{eff}, which is done by bisection in our FORTRAN program. To start a bisection search, lower and upper estimates of the parameter being searched are required. They are obtained in our program, for any order of the approximation, by: (i) adding and subtracting a suitable Δk to an estimate, say k_0, of k_{eff} obtained from a low order (P_1 or P_3) sweep search of k_{eff}, performed between $k = 1$ and the value of k for which the fuel region ceases to be multiplying; (ii) computing the determinant of $\mathbf{M}$ for $k_1 = k_0 - \Delta k$ and $k_2 = k_0 + \Delta k$; and (iii) repeating the procedure with the value of Δk doubled as many times as necessary until a sign change in the values of the determinants computed for k_1 and k_2 is observed. The values of k_1 and k_2 so obtained are taken as the lower and upper estimates of k_{eff} which are needed to start the bisection search. This search is terminated in our program when the search interval has been halved sufficiently many times so that the lower and upper extremes of the interval differ by less than a prescribed amount (10^{-5} was our choice).

In each bisection (or sweep) step, the determinant of $\mathbf{M}$ is computed by means of the LINPACK subroutines DGECO and DGEDI which are based on the LU factorization scheme [27]. When the matrix being factored happens to be close to singular, which is precisely the criticality condition being searched in our program, subroutine DGECO provides an approximate null vector which is used to determine the superposition coefficients of our P_N solutions and consequently our P_N approximations to the scalar flux and current vectors.

Finally, it is important to mention that the use of some special techniques was required in order to make our computational procedure work. In the fuel region, for each bisection (or sweep) step, after the P_N eigenvalues are computed they are ordered (we use the criterion of increasing order in absolute value) and the eigenvectors are normalized (we divide the eigenvectors returned by EISPACK by their Euclidean norm and preserve the sign of the component with largest absolute value in the first calculational step). In the absence of these normalization practices, we have observed that our computational procedure may fail because the pattern of signs displayed by the computed values of $\det \mathbf{M}$ for a monotonic sequence of values of k may become random, as a result of the lack of a consistent eigenvalue ordering and the occurrence of uncontrolled changes in eigenvector normalization during the calculation.

5.2. An Alternative Implementation

Our alternative way of implementing the P_N solution reported in Section 4 is based on the fact that $\mathbf{C}$ and $\mathbf{D}$ are the only submatrices of $\mathbf{M}$ that depend on the properties of the fuel region (see the explicit expressions reported in Appendix A for these and the other submatrices of $\mathbf{M}$). This allows us to reduce the size of the critical determinant from $2J(R-1)$ to J without the need of performing any additional computations during the criticality search, except for a matrix multiplication and a matrix sum per step, both involving matrices of order J.

The basic idea involved in reducing the size of the critical determinant is that of performing backsubstitution in the sequence of equations defined by Eqs. (27a) to (27f). We find that the problem of determining the criticality condition can be reduced to the determination of the (largest) value of k that makes the following homogeneous system of size J have a solution:

$$[\mathbf{D} + \mathbf{P}_2\mathbf{Q}_2^{-1}\mathbf{C}]\mathbf{A}_1 = \mathbf{0}. \tag{32}$$

Here, the matrices $\mathbf{P}_2$ and $\mathbf{Q}_2$ do not depend on the properties of the fuel region and can be computed at the beginning of the calculation, before the criticality search is started. To compute these matrices, we can use the starting values

$$\mathbf{P}_R = \mathbf{F} \tag{33a}$$

and

$$\mathbf{Q}_R = \mathbf{E}, \tag{33b}$$

and the recurrence relations, for $r = R-1, R-2, \ldots, 2$,

$$\mathbf{P}_r = \mathbf{R}_r - \mathbf{S}_r\mathbf{W}_r \tag{34a}$$

and

$$\mathbf{Q}_r = \mathbf{U}_r + \mathbf{V}_r\mathbf{W}_r, \tag{34b}$$

where

$$\mathbf{W}_r = \left[\mathbf{R}_r + \mathbf{P}_{r+1}\mathbf{Q}_{r+1}^{-1}\mathbf{U}_r\right]^{-1}\left[\mathbf{S}_r - \mathbf{P}_{r+1}\mathbf{Q}_{r+1}^{-1}\mathbf{V}_r\right]. \tag{35}$$

Once k_{eff} is determined, $\mathbf{A}_1$, the vector of P_N coefficients in the fuel region, can be assigned to a null vector of the matrix $\mathbf{D} + \mathbf{P}_2\mathbf{Q}_2^{-1}\mathbf{C}$, according to Eq. (32), and the remaining vectors of P_N coefficients can be computed with the help of the recursive scheme defined by

$$\mathbf{A}_r = \begin{cases} \mathbf{Q}_r^{-1}\mathbf{C}\mathbf{A}_{r-1}, & r = 2, \\ \mathbf{Q}_r^{-1}[\mathbf{V}_{r-1}\mathbf{A}_{r-1} + \mathbf{U}_{r-1}\mathbf{B}_{r-1}], & r = 3, 4, \ldots, R, \end{cases} \tag{36a}$$

and

$$\mathbf{B}_r = \mathbf{W}_r\mathbf{A}_r, \quad r = 2, 3, \ldots, R-1. \tag{36b}$$

6. NUMERICAL RESULTS AND DISCUSSION

In this section, we report and discuss the results of the application of our P_N solution to a test problem consisting of a three-region cell which has been used in core studies of a radioisotope producing reactor [28]. The geometry and material composition of the cell are shown in Figure 2. Region 1 ($U_3Si_2 + Al$) is the fuel, region 2 (Al) the cladding, and region 3 (H_2O) the moderator.

The cross-section data for this problem were obtained from the WIMKAL-88 library distributed by the IAEA Nuclear Data Section [29],

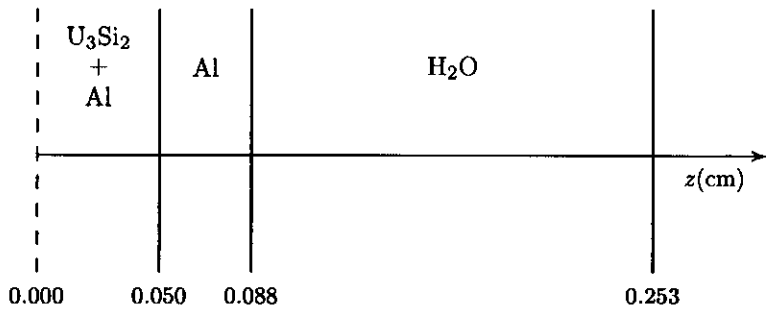

Figure 2. The three-region cell.

which is a nuclear data library of 132 materials in the 69-group WIMS structure. The materials that are present in the cell and their corresponding number densities are listed in Table 1 by region, along with their ID numbers and scattering order in the WIMKAL-88 library. Our initial intention was to use the original data from this library in our calculation. However, in trying this we have detected the occurrence of near degeneracies (i.e., situations where two or more of the P_N eigenvalues become almost, but not exactly, equal). Mathematically speaking, a near degeneracy corresponds to a situation where the eigensystems defined by Eqs. (9) and (13) become near defective.

We note that a recent work [22] has reported a special P_N solution for the case of an exact degeneracy of first order (i.e., a degeneracy involving only two groups) in the slowing-down region. However, the results of that work cannot be used here for two reasons: first, in this work we are not restricted to the slowing-down region; and, second, the degeneracies observed in our problem are not exact and one of them is of third order (i.e., it connects four groups at the same time).

Although this near-degeneracy problem could, in principle, be resolved in a computational manner, using the singular value decomposition approach, as done some years ago for the P_N method applied to radiative transfer with polarization [24], we have decided to avoid this problem by performing a group collapsing of those groups that were causing the problem. Therefore, the three sets of groups defined by groups 16 to 19, groups 20 and 21 and groups 24 and 25 of the original WIMS structure were collapsed into three wider groups, reducing the number of groups in the structure from 69 to 64.

The neutron spectrum used to perform the group collapsing was the infinite-medium transport solution for the homogenized cell reported in

Table 1. Material Composition for the Test Problem

Material	Number density $(\text{b}\cdot\text{cm})^{-1}$	Region	WIMKAL-88 ID#	Scattering order
^{235}U	2.44751×10^{-3}	1	92235	0
^{238}U	9.72708×10^{-3}	1	92238	0
Si	8.11638×10^{-3}	1	14000	0
Al	3.47916×10^{-2}	1	13027	0
^{10}B	2.11594×10^{-7}	1	10	0
Al	6.02439×10^{-2}	2	13027	0
H	6.68589×10^{-2}	3	1011	1
O	3.34299×10^{-2}	3	8016	1

Appendix B. We have found, as discussed in Appendix B, that the group collapsing procedure has not significantly changed the results of our test problem. Nevertheless, a certain degree of ill-conditioning persisted even after we performed the group collapsing: working in double precision on a PC (16 decimal digits), we were able to obtain good results for our test problem only from the full formulation based on Eq. (29); the alternative formulation based on Eq. (32) required the use of double precision on a long-word machine (32 decimal digits) and was not pursued further. To save space, we do not tabulate in this work the 64-group constants that were used in our calculation; anyone interested in obtaining a computer file with these constants may contact the authors.

In Table 2, we report our results for the effective multiplication factor k_{eff}, for several orders of the P_N approximation, and the ANISN results (labeled as S_{N+1}), obtained with the use of 10 mesh intervals per region, completely symmetric quadrature sets that satisfy even moment conditions [23] (except S_{32}, which is based on the Gauss–Legendre quadrature), and convergence criteria of 10^{-4} for k_{eff} and 2×10^{-4} for pointwise angular fluxes in the inner iteration scheme. The choice of the number of mesh intervals used in ANISN was made on the basis that the k_{eff} results did not change when this number was doubled. Thus, starting with 5 mesh intervals per region, we doubled this number to 10, doubled it again to 20, and observed that k_{eff} did not change when we went from 10 to 20 mesh intervals per region. We also show in Table 2 the deviations of the P_N and S_{N+1} results with respect to what we believe to be our best results (the P_{63} results). We can see that the deviations are very similar for both methods, but the P_N deviations are always slightly smaller.

Figures 3 through 5 compare our P_{31} results for the scalar fluxes in groups 1, 22 and 59 with S_{32} results of ANISN. Group 1 is the fastest energy group in the 64-group structure, while group 22 contains the 6.67 eV resonance of ^{238}U and group 59 contains the thermal energy (0.0253 eV). The P_N results were normalized by taking the scalar flux for group 1 equal to 1.0 at

Table 2. The Effective Multiplication Factor k_{eff}

N	P_N	Deviation (%)	S_{N+1}	Deviation (%)
3	1.2381	1.87	1.2376	1.91
7	1.2476	1.12	1.2444	1.37
15	1.2570	0.37	1.2518	0.78
31	1.2608	0.07	1.2605	0.10
47	1.2614	0.02	–	–
63	1.2617	–	–	–

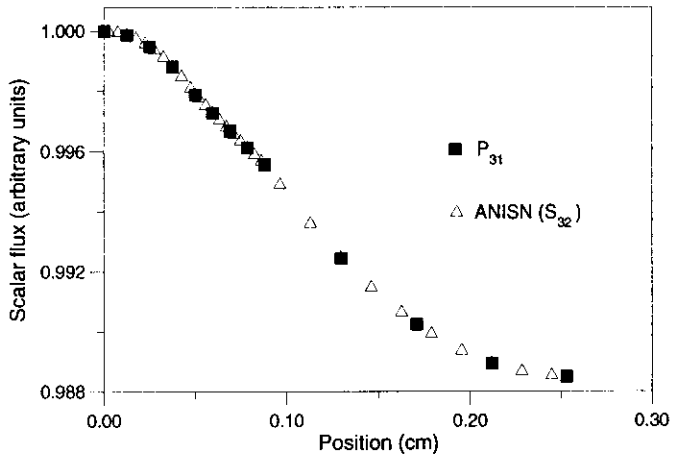

Figure 3. The scalar flux for group 1.

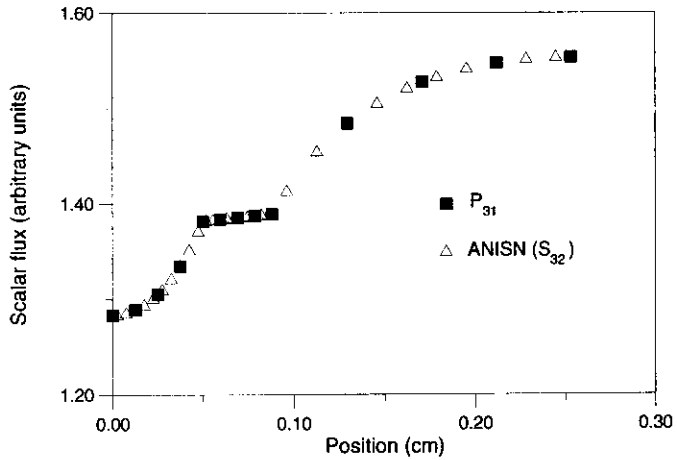

Figure 4. The scalar flux for group 22.

the central point in the fuel ($z = 0$). The ANISN results were normalized by imposing that the P_N and ANISN scalar fluxes for group 1 were the same at the spatial point closest to $z = 0$ in the ANISN grid. It can be observed that the overall agreement between the P_{31} and S_{32} results is quite good.

To provide some benchmark results, we report in Tables 3 and 4 our P_{63} results for the scalar fluxes at the center of the fuel ($z = 0$) and at the right boundary of the moderator region ($z = 0.253$ cm), respectively.

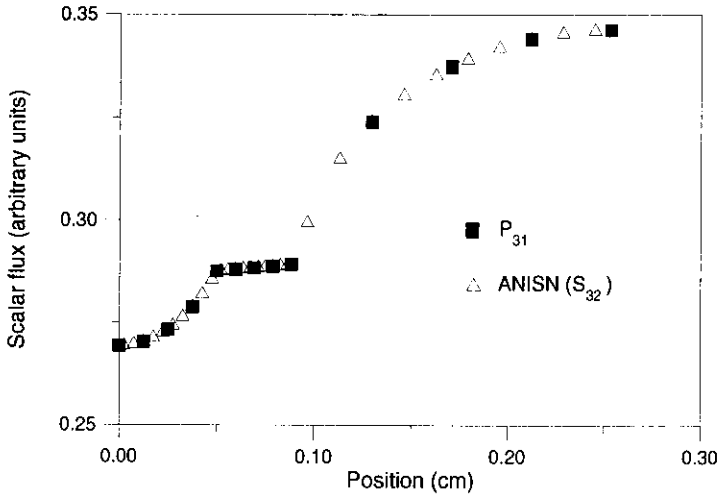

Figure 5. The scalar flux for group 59.

Table 3. The P_{63} Scalar Fluxes at the Center of the Fuel Plate

Group	Flux	Group	Flux	Group	Flux	Group	Flux
1	1.00(+0)[a]	17	5.81(+0)	33	4.76(−2)	49	4.46(−1)
2	4.09(+0)	18	1.99(+0)	34	4.81(−2)	50	6.26(−1)
3	8.48(+0)	19	1.23(+0)	35	4.90(−2)	51	9.69(−1)
4	9.08(+0)	20	2.21(+0)	36	4.72(−2)	52	7.04(−1)
5	8.12(+0)	21	1.09(+0)	37	8.70(−2)	53	5.69(−1)
6	7.04(+0)	22	1.28(+0)	38	1.41(−1)	54	4.47(−1)
7	5.11(+0)	23	3.76(−1)	39	1.79(−1)	55	4.28(−1)
8	4.08(+0)	24	4.76(−1)	40	4.62(−1)	56	4.49(−1)
9	3.23(+0)	25	4.35(−1)	41	4.74(−1)	57	3.99(−1)
10	2.68(+0)	26	6.94(−1)	42	4.67(−1)	58	2.80(−1)
11	2.27(+0)	27	2.99(−1)	43	2.71(−1)	59	2.69(−1)
12	2.11(+0)	28	2.47(−1)	44	1.76(−1)	60	2.47(−1)
13	1.93(+0)	29	4.55(−2)	45	1.26(−1)	61	2.13(−1)
14	1.84(+0)	30	4.49(−2)	46	1.35(−1)	62	1.67(−1)
15	1.77(+0)	31	4.63(−2)	47	2.26(−1)	63	1.06(−1)
16	6.22(+0)	32	4.80(−2)	48	2.65(−1)	64	3.23(−2)

[a]Read as $1.00 \times 10^{+0}$.

Table 4. The P_{63} Scalar Fluxes at the Right Boundary of the Moderator Region

Group	Flux	Group	Flux	Group	Flux	Group	Flux
1	9.79(−1)[a]	17	5.91(+0)	33	4.94(−2)	49	4.86(−1)
2	3.96(+0)	18	2.06(+0)	34	4.97(−2)	50	6.86(−1)
3	8.19(+0)	19	1.30(+0)	35	5.05(−2)	51	1.08(+0)
4	8.68(+0)	20	2.54(+0)	36	4.86(−2)	52	7.99(−1)
5	7.74(+0)	21	1.13(+0)	37	8.94(−2)	53	6.57(−1)
6	6.76(+0)	22	1.54(+0)	38	1.45(−1)	54	5.23(−1)
7	4.92(+0)	23	3.82(−1)	39	1.84(−1)	55	5.09(−1)
8	3.98(+0)	24	4.81(−1)	40	4.75(−1)	56	5.42(−1)
9	3.17(+0)	25	4.38(−1)	41	4.91(−1)	57	4.91(−1)
10	2.65(+0)	26	7.01(−1)	42	4.89(−1)	58	3.53(−1)
11	2.27(+0)	27	3.03(−1)	43	2.88(−1)	59	3.46(−1)
12	2.09(+0)	28	2.54(−1)	44	1.90(−1)	60	3.26(−1)
13	1.94(+0)	29	4.78(−2)	45	1.37(−1)	61	2.93(−1)
14	1.85(+0)	30	4.72(−2)	46	1.48(−1)	62	2.43(−1)
15	1.78(+0)	31	4.85(−2)	47	2.47(−1)	63	1.69(−1)
16	6.24(+0)	32	5.00(−2)	48	2.89(−1)	64	6.65(−2)

[a]Read as 9.79×10^{-1}.

Table 5. The P_{63} Currents at the Fuel-Cladding Interface

Group	Current	Group	Current	Group	Current	Group	Current
1	1.70(−2)[a]	17	−3.13(−2)	33	−5.45(−4)	49	−1.21(−2)
2	7.86(−2)	18	−2.61(−2)	34	−4.91(−4)	50	−1.80(−2)
3	1.52(−1)	19	−2.43(−2)	35	−4.62(−4)	51	−3.33(−2)
4	1.76(−1)	20	−1.27(−1)	36	−4.25(−4)	52	−2.84(−2)
5	1.46(−1)	21	−1.17(−2)	37	−7.27(−4)	53	−2.61(−2)
6	9.91(−2)	22	−1.03(−1)	38	−1.10(−3)	54	−2.26(−2)
7	6.01(−2)	23	−2.26(−3)	39	−1.55(−3)	55	−2.38(−2)
8	3.03(−2)	24	−1.96(−3)	40	−3.84(−3)	56	−2.75(−2)
9	1.80(−2)	25	−1.04(−3)	41	−5.04(−3)	57	−2.72(−2)
10	8.60(−3)	26	−2.34(−3)	42	−6.50(−3)	58	−2.11(−2)
11	1.74(−3)	27	−1.07(−3)	43	−5.38(−3)	59	−2.23(−2)
12	2.95(−3)	28	−2.05(−3)	44	−4.45(−3)	60	−2.30(−2)
13	−5.15(−4)	29	−7.33(−4)	45	−3.55(−3)	61	−2.29(−2)
14	−1.21(−3)	30	−7.38(−4)	46	−4.02(−3)	62	−2.16(−2)
15	−2.72(−3)	31	−6.93(−4)	47	−6.71(−3)	63	−1.81(−2)
16	−9.84(−3)	32	−6.23(−4)	48	−7.47(−3)	64	−9.57(−3)

[a]Read as 1.70×10^{-2}.

Table 6. The P_{63} Currents at the Cladding-Moderator Interface

Group	Current	Group	Current	Group	Current	Group	Current
1	1.47(−2)[a]	17	−3.13(−2)	33	−5.48(−4)	49	−1.22(−2)
2	7.14(−2)	18	−2.60(−2)	34	−4.95(−4)	50	−1.81(−2)
3	1.44(−1)	19	−2.42(−2)	35	−4.66(−4)	51	−3.36(−2)
4	1.75(−1)	20	−1.27(−1)	36	−4.30(−4)	52	−2.86(−2)
5	1.49(−1)	21	−1.18(−2)	37	−7.38(−4)	53	−2.62(−2)
6	1.03(−1)	22	−1.03(−1)	38	−1.12(−3)	54	−2.28(−2)
7	6.34(−2)	23	−2.38(−3)	39	−1.57(−3)	55	−2.39(−2)
8	3.28(−2)	24	−2.00(−3)	40	−3.89(−3)	56	−2.77(−2)
9	1.92(−2)	25	−1.07(−3)	41	−5.09(−3)	57	−2.73(−2)
10	1.11(−2)	26	−2.39(−3)	42	−6.54(−3)	58	−2.12(−2)
11	1.11(−4)	27	−1.10(−3)	43	−5.40(−3)	59	−2.24(−2)
12	5.89(−3)	28	−2.05(−3)	44	−4.46(−3)	60	−2.31(−2)
13	−6.73(−4)	29	−7.29(−4)	45	−3.56(−3)	61	−2.31(−2)
14	−1.36(−3)	30	−7.36(−4)	46	−4.03(−3)	62	−2.17(−2)
15	−4.29(−3)	31	−6.93(−4)	47	−6.74(−3)	63	−1.82(−2)
16	−8.39(−3)	32	−6.25(−4)	48	−7.51(−3)	64	−9.62(−3)

[a]Read as 1.47×10^{-2}.

In addition, we report in Tables 5 and 6 our P_{63} results for the currents at the fuel-cladding interface ($z = 0.050$ cm) and at the cladding-moderator interface ($z = 0.088$ cm), respectively. These results are thought to be accurate, in general, to within ± 1 in the last figure shown.

The P_N calculations for $N = 3$, 7 and 15 and the ANISN calculations were done on a PC equipped with a 100-MHz Pentium processor and 64 MB of RAM; the P_{31}, P_{47} and P_{63} calculations were done on a 350-MHz Pentium II machine with 512 MB of RAM.

In regard to computer time, the ANISN calculations were, for N varying between 3 and 15, from one to three orders of magnitude more efficient than the P_N calculations, due to the simplification allowed by the use of the spatial discretization scheme on which ANISN is based. In fact, because the cell is optically thin for all energy groups, it was possible to obtain good results using a relatively small number of mesh intervals per region in ANISN. This difference in computational performance could be substantially reduced if the alternative P_N implementation discussed in Section 5 could be used for this problem.

Finally, to close this section, we would like to mention that we have also used the Marshak prescription [1] for generating the approximate P_N interface conditions required in Section 4. The Marshak prescription is based

on multiplying the boundary or interface conditions by $P_{2i-1}(\mu)$, $i = 1, 2, \ldots, I = (N+1)/2$, and integrating over μ in the appropriate half-range interval. It turns out that the only modification needed in our analysis to accommodate the use of the Marshak interface conditions is the replacement of $P_n(\mu_i)$ by $S_{i-1,n}$, where

$$S_{i-1,n} = \int_0^1 P_{2i-1}(\mu) P_n(\mu)\, d\mu, \tag{37}$$

in Eqs. (A.2) and (A.4) of Appendix A. The constants $S_{i-1,n}$ defined by Eq. (37) and required for $i = 1, 2, \ldots, I$ and $n = 0, 1, \ldots, N$ can be easily computed by recurrence [30, 31]. Our conclusion was that the quality of the numerical results obtained for the test problem when the Marshak interface conditions were used is very similar to the quality of the Mark results.

7. CONCLUDING REMARKS

In this work, we have developed and implemented the P_N method for cell calculations of plate-type fuel assemblies. Having extended the class of criticality problems to which the P_N method can be successfully applied, we concluded from our work that cell calculations are more demanding than assembly calculations, in the sense that they require a much higher order of approximation, say $N > 30$, as compared to the $N < 10$ approximations typically used in assembly calculations [19]. Since the modifications that need to be introduced into our P_N solution to enable its application to criticality problems in assemblies are minimal, we plan to investigate this class of problems in a future work.

To conclude, we would like to comment briefly on the possible existence of more than one physically acceptable value of k_{eff} in the solution of criticality problems. This possibility has been mentioned in the literature [4], and in such a case the relevant k_{eff} would be the largest one since it corresponds to the configuration of minimum critical mass. Recently, in our continuing work on critical problems [32], we have encountered a two-group problem for which the critical determinant can be zero for more than one value of the multiplication factor k in a very conspicuous way. Investigating numerically the solutions associated with the four largest values of k for this problem, we have found that only the largest one gives rise to strictly positive scalar fluxes throughout the system and, thus, to a physically acceptable solution. Whether or not this is true in general for criticality problems in multigroup transport theory is still an open question.

APPENDIX A

The Submatrices of M

We start this appendix by noting that all of the $J \times J$ submatrices **C**, **D**, **E**, **F**, and $\mathbf{U}_r, \mathbf{V}_r, \mathbf{R}_r, \mathbf{S}_r, r = 2, 3, \ldots, R-1$, of the matrix **M** defined by Eq. (30) have a similar structure based on constituent vectors of dimension G. For example, submatrix **C** can be written as

$$\mathbf{C} = \begin{pmatrix} \mathbf{c}_{11} & \mathbf{c}_{12} & \cdots & \mathbf{c}_{1J} \\ \mathbf{c}_{21} & \mathbf{c}_{22} & \cdots & \mathbf{c}_{2J} \\ \vdots & \vdots & \ddots & \vdots \\ \mathbf{c}_{I1} & \mathbf{c}_{I2} & \cdots & \mathbf{c}_{IJ} \end{pmatrix}, \tag{A.1}$$

where we recall that $I = (N+1)/2$. In Eq. (A.1), each of the vectors $\mathbf{c}_{ij}$, $i = 1, 2, \ldots, I$ and $j = 1, 2, \ldots, J$, has dimension G and can be expressed, if we observe the eigenvalue ordering used in Section 4 and introduce the definition

$$\mathbf{T}^e_{r,i}(\xi_{r,j}) = \sum_{\substack{n=0 \\ n \text{ even}}}^{N-1} (2n+1) P_n(\mu_i) \mathbf{G}_{r,n}(\xi_{r,j}), \tag{A.2}$$

as

$$\mathbf{c}_{ij} = \cos(\tau_1/\eta_{1,j})\, \Re\{\mathbf{T}^e_{1,i}(\xi_{1,j})\}, \tag{A.3a}$$

for $j = 1, 2, \ldots, J_I$,

$$\mathbf{c}_{ij} = \left(1 + e^{-2\tau_1/\xi_{1,j}}\right) \mathbf{T}^e_{1,i}(\xi_{1,j}), \tag{A.3b}$$

for $j = J_I + 1, J_I + 2, \ldots, J_I + J_R$,

$$\mathbf{c}_{ij} = \left[1 + e^{-2\lambda_{1,j}\tau_1/(\xi_{1,j}\bar{\xi}_{1,j})}\right] \cos\left[\eta_{1,j}\tau_1/(\xi_{1,j}\bar{\xi}_{1,j})\right] \Re\{\mathbf{T}^e_{1,i}(\xi_{1,j})\} + \left[1 - e^{-2\lambda_{1,j}\tau_1/(\xi_{1,j}\bar{\xi}_{1,j})}\right] \sin\left[\eta_{1,j}\tau_1/(\xi_{1,j}\bar{\xi}_{1,j})\right] \Im\{\mathbf{T}^e_{1,i}(\xi_{1,j})\}, \tag{A.3c}$$

for $j = J_I + J_R + 1, J_I + J_R + 3, \ldots, J_I + J_R + 2J_C - 1$, and

$$\mathbf{c}_{ij} = \left[1 + e^{-2\lambda_{1,j}\tau_1/(\xi_{1,j}\bar{\xi}_{1,j})}\right] \cos\left[\eta_{1,j}\tau_1/(\xi_{1,j}\bar{\xi}_{1,j})\right] \Im\{\mathbf{T}^e_{1,i}(\xi_{1,j})\} - \left[1 - e^{-2\lambda_{1,j}\tau_1/(\xi_{1,j}\bar{\xi}_{1,j})}\right] \sin\left[\eta_{1,j}\tau_1/(\xi_{1,j}\bar{\xi}_{1,j})\right] \Re\{\mathbf{T}^e_{1,i}(\xi_{1,j})\}, \tag{A.3d}$$

for $j = J_I + J_R + 2, J_I + J_R + 4, \ldots, J_I + J_R + 2J_C$.

Since as mentioned before the other submatrices in Eq. (30) have the same type of structure displayed by Eq. (A.1), we only list here the definitions of their constituent vectors of dimension G. Beginning with submatrix **D**, we use the definition

$$\mathbf{T}^o_{r,i}(\xi_{r,j}) = \sum_{\substack{n=1 \\ n \text{ odd}}}^{N} (2n+1) P_n(\mu_i) \mathbf{G}_{r,n}(\xi_{r,j}), \tag{A.4}$$

to write the constituent vector $\mathbf{d}_{ij}$ for this submatrix as

$$\mathbf{d}_{ij} = \sin(\tau_1/\eta_{1,j})\, \Im\{\mathbf{T}^o_{1,i}(\xi_{1,j})\}, \tag{A.5a}$$

for $j = 1, 2, \ldots, J_I$,

$$\mathbf{d}_{ij} = \left(1 - e^{-2\tau_1/\xi_{1,j}}\right) \mathbf{T}^o_{1,i}(\xi_{1,j}), \tag{A.5b}$$

for $j = J_I + 1, J_I + 2, \ldots, J_I + J_R$,

$$\mathbf{d}_{ij} = \left[1 - e^{-2\lambda_{1,j}\tau_1/(\xi_{1,j}\bar{\xi}_{1,j})}\right] \cos\left[\eta_{1,j}\tau_1/(\xi_{1,j}\bar{\xi}_{1,j})\right] \Re\{\mathbf{T}^o_{1,i}(\xi_{1,j})\} + \left[1 + e^{-2\lambda_{1,j}\tau_1/(\xi_{1,j}\bar{\xi}_{1,j})}\right] \sin\left[\eta_{1,j}\tau_1/(\xi_{1,j}\bar{\xi}_{1,j})\right] \Im\{\mathbf{T}^o_{1,i}(\xi_{1,j})\}, \tag{A.5c}$$

for $j = J_I + J_R + 1, J_I + J_R + 3, \ldots, J_I + J_R + 2J_C - 1$, and

$$\mathbf{d}_{ij} = \left[1 - e^{-2\lambda_{1,j}\tau_1/(\xi_{1,j}\bar{\xi}_{1,j})}\right] \cos\left[\eta_{1,j}\tau_1/(\xi_{1,j}\bar{\xi}_{1,j})\right] \Im\{\mathbf{T}^o_{1,i}(\xi_{1,j})\} - \left[1 + e^{-2\lambda_{1,j}\tau_1/(\xi_{1,j}\bar{\xi}_{1,j})}\right] \sin\left[\eta_{1,j}\tau_1/(\xi_{1,j}\bar{\xi}_{1,j})\right] \Re\{\mathbf{T}^o_{1,i}(\xi_{1,j})\}, \tag{A.5d}$$

for $j = J_I + J_R + 2, J_I + J_R + 4, \ldots, J_I + J_R + 2J_C$. This completes the definition of the submatrices that depend on the properties of the fuel region.

Now, for an intermediate region $2 \le r \le R-1$, the constituent vectors of dimension G for the submatrices $\mathbf{U}_r$, $\mathbf{V}_r$, $\mathbf{R}_r$, and $\mathbf{S}_r$ are defined, respectively, as

$$\mathbf{u}^r_{ij} = \mathbf{T}^e_{r,i}(\xi_{r,j}), \tag{A.6a}$$

$$\mathbf{v}^r_{ij} = e^{-(\tau_r - \tau_{r-1})/\xi_{r,j}} \mathbf{T}^e_{r,i}(\xi_{r,j}), \tag{A.6b}$$

$$\mathbf{r}^r_{ij} = \mathbf{T}^o_{r,i}(\xi_{r,j}), \tag{A.6c}$$

and

$$\mathbf{s}^r_{ij} = e^{-(\tau_r - \tau_{r-1})/\xi_{r,j}} \mathbf{T}^o_{r,i}(\xi_{r,j}), \tag{A.6d}$$

for $j = 1, 2, \ldots, J_R$,

$$\mathbf{u}^r_{ij} = \Re\{\mathbf{T}^e_{r,i}(\xi_{r,j})\}, \tag{A.6e}$$

$$\mathbf{v}_{ij}^{r} = e^{-\lambda_{r,j}(\tau_r-\tau_{r-1})/(\xi_{r,j}\bar{\xi}_{r,j})}\Big\{\cos\big[\eta_{r,j}(\tau_r-\tau_{r-1})/(\xi_{r,j}\bar{\xi}_{r,j})\big]\,\Re\{\mathbf{T}_{r,i}^{e}(\xi_{r,j})\} - \sin\big[\eta_{r,j}(\tau_r-\tau_{r-1})/(\xi_{r,j}\bar{\xi}_{r,j})\big]\,\Im\{\mathbf{T}_{r,i}^{e}(\xi_{r,j})\}\Big\}, \tag{A.6f}$$

$$\mathbf{r}_{ij}^{r} = \Re\{\mathbf{T}_{r,i}^{o}(\xi_{r,j})\}, \tag{A.6g}$$

and

$$\mathbf{s}_{ij}^{r} = e^{-\lambda_{r,j}(\tau_r-\tau_{r-1})/(\xi_{r,j}\bar{\xi}_{r,j})}\Big\{\cos\big[\eta_{r,j}(\tau_r-\tau_{r-1})/(\xi_{r,j}\bar{\xi}_{r,j})\big]\,\Re\{\mathbf{T}_{r,i}^{o}(\xi_{r,j})\} - \sin\big[\eta_{r,j}(\tau_r-\tau_{r-1})/(\xi_{r,j}\bar{\xi}_{r,j})\big]\,\Im\{\mathbf{T}_{r,i}^{o}(\xi_{r,j})\}\Big\}, \tag{A.6h}$$

for $j = J_R+1, J_R+3, \ldots, J_R+2J_C-1$, and

$$\mathbf{u}_{ij}^{r} = \Im\{\mathbf{T}_{r,i}^{e}(\xi_{r,j})\}, \tag{A.6i}$$

$$\mathbf{v}_{ij}^{r} = e^{-\lambda_{r,j}(\tau_r-\tau_{r-1})/(\xi_{r,j}\bar{\xi}_{r,j})}\Big\{\sin\big[\eta_{r,j}(\tau_r-\tau_{r-1})/(\xi_{r,j}\bar{\xi}_{r,j})\big]\,\Re\{\mathbf{T}_{r,i}^{e}(\xi_{r,j})\} + \cos\big[\eta_{r,j}(\tau_r-\tau_{r-1})/(\xi_{r,j}\bar{\xi}_{r,j})\big]\,\Im\{\mathbf{T}_{r,i}^{e}(\xi_{r,j})\}\Big\}, \tag{A.6j}$$

$$\mathbf{r}_{ij}^{r} = \Im\{\mathbf{T}_{r,i}^{o}(\xi_{r,j})\}, \tag{A.6k}$$

and

$$\mathbf{s}_{ij}^{r} = e^{-\lambda_{r,j}(\tau_r-\tau_{r-1})/(\xi_{r,j}\bar{\xi}_{r,j})}\Big\{\sin\big[\eta_{r,j}(\tau_r-\tau_{r-1})/(\xi_{r,j}\bar{\xi}_{r,j})\big]\,\Re\{\mathbf{T}_{r,i}^{o}(\xi_{r,j})\} + \cos\big[\eta_{r,j}(\tau_r-\tau_{r-1})/(\xi_{r,j}\bar{\xi}_{r,j})\big]\,\Im\{\mathbf{T}_{r,i}^{o}(\xi_{r,j})\}\Big\}, \tag{A.6l}$$

for $j = J_R+2, J_R+4, \ldots, J_R+2J_C$.

Finally, for the outermost region, the constituent vectors of dimension G for the submatrices **E** and **F** are defined, respectively, as

$$\mathbf{e}_{ij} = \Big[1 + e^{-2(\tau_R-\tau_{R-1})/\xi_{R,j}}\Big]\mathbf{T}_{R,i}^{e}(\xi_{R,j}) \tag{A.7a}$$

and

$$\mathbf{f}_{ij} = \Big[1 - e^{-2(\tau_R-\tau_{R-1})/\xi_{R,j}}\Big]\mathbf{T}_{R,i}^{o}(\xi_{R,j}), \tag{A7b}$$

for $j = 1, 2, \ldots, J_R$,

$$\mathbf{e}_{ij} = \Re\{\mathbf{T}_{R,i}^{e}(\xi_{R,j})\} + e^{-2\lambda_{R,j}(\tau_R-\tau_{R-1})/(\xi_{R,j}\bar{\xi}_{R,j})} \times \Big\{\cos\big[2\eta_{R,j}(\tau_R-\tau_{R-1})/(\xi_{R,j}\bar{\xi}_{R,j})\big]\,\Re\{\mathbf{T}_{R,i}^{e}(\xi_{R,j})\} - \sin\big[2\eta_{R,j}(\tau_R-\tau_{R-1})/(\xi_{R,j}\bar{\xi}_{R,j})\big]\,\Im\{\mathbf{T}_{R,i}^{e}(\xi_{R,j})\}\Big\} \tag{A.7c}$$

and

$$\mathbf{f}_{ij} = \Re\{\mathbf{T}_{R,i}^{o}(\xi_{R,j})\} - e^{-2\lambda_{R,j}(\tau_R-\tau_{R-1})/(\xi_{R,j}\bar{\xi}_{R,j})} \times \Big\{\cos\big[2\eta_{R,j}(\tau_R-\tau_{R-1})/(\xi_{R,j}\bar{\xi}_{R,j})\big]\,\Re\{\mathbf{T}_{R,i}^{o}(\xi_{R,j})\} - \sin\big[2\eta_{R,j}(\tau_R-\tau_{R-1})/(\xi_{R,j}\bar{\xi}_{R,j})\big]\,\Im\{\mathbf{T}_{R,i}^{o}(\xi_{R,j})\}\Big\}, \tag{A.7d}$$

for $j = J_R+1, J_R+3, \ldots, J_R+2J_C-1$, and

$$\mathbf{e}_{ij} = \Im\{\mathbf{T}_{R,i}^{e}(\xi_{R,j})\} + e^{-2\lambda_{R,j}(\tau_R-\tau_{R-1})/(\xi_{R,j}\bar{\xi}_{R,j})} \times \Big\{\sin\big[2\eta_{R,j}(\tau_R-\tau_{R-1})/(\xi_{R,j}\bar{\xi}_{R,j})\big]\,\Re\{\mathbf{T}_{R,i}^{e}(\xi_{R,j})\} + \cos\big[2\eta_{R,j}(\tau_R-\tau_{R-1})/(\xi_{R,j}\bar{\xi}_{R,j})\big]\,\Im\{\mathbf{T}_{R,i}^{e}(\xi_{R,j})\}\Big\} \tag{A.7e}$$

and

$$\mathbf{f}_{ij} = \Im\{\mathbf{T}_{R,i}^{o}(\xi_{R,j})\} - e^{-2\lambda_{R,j}(\tau_R-\tau_{R-1})/(\xi_{R,j}\bar{\xi}_{R,j})} \times \Big\{\sin\big[2\eta_{R,j}(\tau_R-\tau_{R-1})/(\xi_{R,j}\bar{\xi}_{R,j})\big]\,\Re\{\mathbf{T}_{R,i}^{o}(\xi_{R,j})\} + \cos\big[2\eta_{R,j}(\tau_R-\tau_{R-1})/(\xi_{R,j}\bar{\xi}_{R,j})\big]\,\Im\{\mathbf{T}_{R,i}^{o}(\xi_{R,j})\}\Big\}, \tag{A.7f}$$

for $j = J_R+2, J_R+4, \ldots, J_R+2J_C$.

To close this appendix, we note that the reason why we have used the combinations of Eq. (25) expressed by Eq. (26) to define our interface conditions in Section 4 now becomes apparent: the summations in Eqs. (A.2) and (A.4) involve only half the number of terms than they would if these combinations had not been used.

APPENDIX B

The Spectrum Used in the Group Collapsing Procedure

In this appendix, we report our way of defining the neutron spectrum used to perform the data collapsing from 69 to 64 groups for the test problem described in Section 6. In order to approximate as much as possible the actual spectrum in the cell, we elected to use the infinite-medium solution for the equivalent homogenized cell as our collapsing spectrum. Therefore, we computed the dominant eigenvalue k_∞, which can be viewed as a multigroup alternative to the parameter k_{BMS} introduced in two-group transport

theory [33, 34], and the dominant eigenvector Ψ_∞ of the eigensystem

$$(\mathbf{S} - \mathbf{T}_s)^{-1}\mathbf{T}_f\Psi = k\Psi, \tag{B.1}$$

obtained by neglecting the streaming term in Eq. (1) and recognizing that only the isotropic component of the transfer matrix plays a role in the infinite medium solution for the homogenized cell. In Eq. (B.1), $\mathbf{S}$ is a diagonal matrix that contains the group total cross sections $\{s_i\}$ for the homogenized cell in the diagonal and the scattering and fission matrices $\mathbf{T}_s$ and $\mathbf{T}_f$ have as elements, respectively, the group constants $\{\sigma_{s,ij}(0)\}$ and $\{\chi_i(\nu\sigma_f)_j\}$ for the homogenized cell.

We have used the sequence of EISPACK routines mentioned in Section 3 and the original cross-section data in 69 groups from the WIMKAL-88 library to find $k_\infty = 1.2333$ and the corresponding components of the eigenvector Ψ_∞ listed in Table B.1, which were then used as the collapsing

Table B.1. The Components of the Dominant Eigenvector Ψ_∞

i	$\Psi_{\infty,i}$	i	$\Psi_{\infty,i}$	i	$\Psi_{\infty,i}$
1	1.0000(+0)[a]	24	1.2680(+0)	47	4.4336(−1)
2	3.9905(+0)	25	1.0439(+0)	48	2.6005(−1)
3	8.1510(+0)	26	1.0499(+0)	49	1.7056(−1)
4	8.5227(+0)	27	1.3452(+0)	50	1.2250(−1)
5	7.5439(+0)	28	3.4934(−1)	51	1.3186(−1)
6	6.5484(+0)	29	4.4020(−1)	52	2.2020(−1)
7	4.7516(+0)	30	4.0111(−1)	53	2.5723(−1)
8	3.8332(+0)	31	6.4148(−1)	54	4.2866(−1)
9	3.0475(+0)	32	2.7683(−1)	55	5.9454(−1)
10	2.5380(+0)	33	2.3145(−1)	56	9.0682(−1)
11	2.1797(+0)	34	4.3311(−2)	57	6.4997(−1)
12	2.0007(+0)	35	4.2750(−2)	58	5.2273(−1)
13	1.8536(+0)	36	4.4012(−2)	59	4.0893(−1)
14	1.7686(+0)	37	4.5447(−2)	60	3.9112(−1)
15	1.7063(+0)	38	4.4939(−2)	61	4.0999(−1)
16	1.5275(+0)	39	4.5241(−2)	62	3.6443(−1)
17	1.4994(+0)	40	4.5988(−2)	63	2.5709(−1)
18	1.4824(+0)	41	4.4232(−2)	64	2.4742(−1)
19	1.4652(+0)	42	8.1457(−2)	65	2.2873(−1)
20	2.8757(+0)	43	1.3209(−1)	66	2.0054(−1)
21	2.7646(+0)	44	1.6739(−1)	67	1.6051(−1)
22	1.9576(+0)	45	4.3266(−1)	68	1.0689(−1)
23	1.2260(+0)	46	4.4608(−1)	69	3.8565(−2)

[a]Read as $1.0000 \times 10^{+0}$.

spectrum in 69 groups to define the 64-group cross-section data for the problem solved in Section 6. The dominant eigenvector was normalized by taking its first component equal to 1.0. It should be noted that all of the other eigenvalues of $(\mathbf{S} - \mathbf{T}_s)^{-1}\mathbf{T}_f$ appeared clustered around zero in our EISPACK solutions.

Finally, to test the effect of the collapsing procedure in the solution, we have used the ANISN code to solve the problem of Section 6 with group constants defined in both the 69- and the 64-group structures. Since the values for the effective multiplication factor obtained from our S_4 calculations were, respectively, $k_{\text{eff}} = 1.2378$ and $k_{\text{eff}} = 1.2376$, we have concluded that the group collapsing procedure did not significantly affect the results of our test problem.

ACKNOWLEDGMENTS

One of the authors (A.D.C.) is grateful to the Ministry of Science and Technology (RHAE program) for the financial support that allowed him to pursue his doctoral degree. The other author (R.D.M.G.) wishes to express his sincere gratitude to Farzad Rahnema and the Georgia Institute of Technology for partial support that made possible for him to attend the XVI ICTT. The authors also wish to thank A. C. C. Migliano, coordinator of the CTA/IEAv/EFA-E Electromagnetic Systems Laboratory, for computational resources that were used to run some time- and memory-intensive calculations, A. F. Dias for his help in the implementation of the computer program, E. S. Chalhoub and R. Matheus for their expert advice on LaTeX, and D. K. Parsons for a helpful comment. The work of R.D.M.G. was partially supported by CNPq.

REFERENCES

1. Davison, B. *Neutron Transport Theory*; Oxford University Press: London, 1957.
2. Weinberg, A. M.; Wigner, E. P. *The Physical Theory of Neutron Chain Reactors*; The University of Chicago Press: Chicago, IL, 1958.
3. Kofink, W. Recent Developments in the Spherical Harmonics Method and New Integral Solutions of the Boltzmann Equation in Spherical Geometry. In *Developments in Transport Theory*; Inönü, E., Zweifel, P. F., Eds.; Academic Press: London, 1967; 149–212.
4. Bell, G. I.; Glasstone, S. *Nuclear Reactor Theory*; Van Nostrand Reinhold: New York, 1970.

5. Marshak, R. E. Note on the Spherical Harmonics Method as Applied to the Milne Problem for a Sphere. Phys. Rev. **1947**, *71*, 443–446.
6. Mark, J. C. *The Spherical Harmonics II*, Report MT-97; National Research Council of Canada, Atomic Energy Project: Ottawa, Canada, 1945.
7. Pomraning, G. C. Variational Boundary Conditions for the Spherical Harmonics Approximation to the Neutron Transport Equation. Ann. Phys. **1964**, *27*, 193–215.
8. Pomraning, G. C. A Generalized Approximation for Neutron Transport Problems. Nukleonik **1964**, *6*, 348–356.
9. Federighi, F. D. Vacuum Boundary Conditions for the Spherical Harmonics Method. Nukleonik **1964**, *6*, 278–285.
10. Neshat, K.; Siewert, C. E.; Ishiguro, Y. An Improved *P-L* Solution to the Reflected Critical-Reactor Problem in Slab Geometry. Nucl. Sci. Eng. **1977**, *62*, 330–332.
11. Ganguly, K.; Sengupta, A. A Transport Theoretic P_N Approximation. Nucl. Sci. Eng. **1980**, *74*, 1–12.
12. Ganguly, K.; Sengupta, A. Interface and Source Problems by a Transport Theoretic P_N Approximation. Nucl. Sci. Eng. **1981**, *77*, 13–19.
13. Aronson, R. Subcritical Problems in Spherical Geometry. Nucl. Sci. Eng. **1984**, *86*, 136–149.
14. Aronson, R. Critical Problems for Bare and Reflected Slabs and Spheres. Nucl. Sci. Eng. **1984**, *86*, 150–156.
15. Lee, C. E.; Dias, M. P. Analytical Solutions to the Moment Transport Equations – I: One-Group One-Region Slab and Sphere Criticality. Ann. Nucl. Energy **1984**, *11*, 515–530.
16. Larsen, E. W.; Pomraning, G. C. The P_N Theory as an Asymptotic Limit of Transport Theory in Planar Geometry – I: Analysis. Nucl. Sci. Eng. **1991**, *109*, 49–75.
17. Rulko, R. P.; Larsen, E. W.; Pomraning, G. C. The P_N Theory as an Asymptotic Limit of Transport Theory in Planar Geometry – II: Numerical Results. Nucl. Sci. Eng. **1991**, *109*, 76–85.
18. Garcia, R. D. M.; Siewert, C. E. A Stable Shifted-Legendre Projection Scheme for Generating P_N Boundary Conditions. Ann. Nucl. Energy **1996**, *23*, 321–332.
19. Lee, C. E.; Fan, W. C. P.; Dias, M. P. Analytical Solutions to the Moment Transport Equations – II: Multiregion, Multigroup 1-D Slab, Cylinder and Sphere Criticality and Source Problems. Ann. Nucl. Energy **1985**, *12*, 613–632.

20. Siewert, C. E. A Spherical-Harmonics Method for Multi-Group or Non-Gray Radiation Transport. J. Quant. Spectrosc. Radiat. Transfer **1993**, *49*, 95–106.
21. Caldeira, A. D.; Dias, A. F.; Garcia, R. D. M. A P_N Solution to the Multigroup Slowing-Down Problem – I: Basic Formulation. Nucl. Sci. Eng. **1998**, *130*, 60–69.
22. Caldeira, A. D.; Dias, A. F.; Garcia, R. D. M. A P_N Solution to the Multigroup Slowing-Down Problem – II: The Degenerate Case. Nucl. Sci. Eng. **1998**, *130*, 70–78.
23. Engle Jr., W. W. *A Users Manual for ANISN, a One Dimensional Discrete Ordinates Transport Code with Anisotropic Scattering*, Report K-1693 (Updated); Union Carbide, Nuclear Division, 1973.
24. Garcia, R. D. M.; Siewert, C. E. A Generalized Spherical Harmonics Solution for Radiative Transfer Models that Include Polarization Effects. J. Quant. Spectrosc. Radiat. Transfer **1986**, *36*, 401–423.
25. Siewert, C. E.; Thomas, Jr., J. R. A Method for Computing the Discrete Spectrum Basic to Multi-Group Transport Theory. J. Quant. Spectrosc. Radiat. Transfer **1987**, *37*, 111–115.
26. Smith, B. T.; Boyle, J. M.; Dongarra, J. J.; Garbow, B. S.; Ikebe, Y.; Klema, V. C.; Moler, C. B. *Matrix Eigensystem Routines – EISPACK Guide*; Springer-Verlag: Berlin, 1976.
27. Dongarra, J. J.; Bunch, J. R.; Moler, C. B.; Stewart, G. W. *LINPACK Users' Guide*; SIAM: Philadelphia, PA, 1979.
28. Batista, J. L.; Renke, C. A. C. Nova Concepção do Núcleo do Reator Produtor de Radioisótopos Utilizando o Combustível U_3Si_2-Al. Proc. V General Congress of Nuclear Energy, Rio de Janeiro, Brazil, Aug. 28–Sept. 2, 1994; Associação Brasileira de Energia Nuclear: Rio de Janeiro, Brazil, 1994.
29. Kim, J.-D. *WIMKAL-88, the 1988 Version of the WIMS-KAERI Library*, Report IAEA-NDS-98; IAEA Nuclear Data Section: Vienna, 1990.
30. Benassi, M.; Cotta, R. M.; Siewert, C. E. The P_N Method for Radiative Transfer Problems with Reflective Boundary Conditions. J. Quant. Spectrosc. Radiat. Transfer **1983**, *30*, 547–553.
31. Benassi, M.; Garcia, R. D. M.; Karp, A. H.; Siewert, C. E. A High-Order Spherical Harmonics Solution to the Standard Problem in Radiative Transfer. Astrophys. J. **1984**, *280*, 853–864.
32. Caldeira, A. D.; Garcia, R. D. M. On Criticality Calculations in Multislab Geometry. Ann. Nucl. Energy **2001**, *28*, 1563 1581.
33. Burniston, E. E.; Mullikin, T. W.; Siewert, C. E. Steady-State Solutions in the Two-Group Theory of Neutron Diffusion. J. Math. Phys. **1972**, *13*, 1461–1465.

34. Kriese, J. T.; Siewert, C. E.; Yener, Y. Two-Group Critical Problems for Slabs and Spheres in Neutron-Transport Theory. Nucl. Sci. Eng. **1973**, *50*, 3–9.

Received August 4, 1999
Revised May 29, 2000
Accepted May 29, 2000

DIFFUSION A
OF RADIAT
EQUATIONS

Gui

Departmen
University of Chi
E-mail: gbal

Al

We address the propagatio
earthquake in the earth cr
from the atmosphere and
faces. Geophysical studies
transfer in this frequency
energy density of seismic
distances, radiative transf
be approximated by a diff
ness of the crust is of th
path, the average distanc
number ν to be scattered i
action with the inhomog
there cannot be diffusio
paper shows that diffus
sense. The radiative tran
in the limit of vanishing
two-dimensional diffusio
and a one-dimensional tr